Journal of Sol-Gel Science and Technology (2020) 93:291–301
https://doi.org/10.1007/s10971-019-05197-8

ORIGINAL PAPER: NANO-STRUCTURED MATERIALS (PARTICLES, FIBERS, COLLOIDS, COMPOSITES, ETC.)

Check for updates

Synthesis of Ag–Carbon–TiO_2 composite tubes and their antibacterial and organic degradation properties

Lijun Ji[1] · Xiang Qin[1] · Jingjing Zheng[1] · Shu Zhou[1] · Tong Xu[1] · Guojun Shi[1]

Received: 4 September 2019 / Accepted: 19 November 2019 / Published online: 30 November 2019

Abstract

Ag–Carbon–TiO_2 composite tubes were prepared by using polystyrene/$AgNO_3$ composite fibers as a sacrifice template and a co-pyrolysis process. The Ag–Carbon–TiO_2 tubes were characterized by SEM, TEM, X-ray diffraction, Raman spectrum, XPS, and UV–vis spectrum. The results showed that the Ag–Carbon–TiO_2 tubes possessed uniform tubular structure with amorphous carbon, graphitic carbon, and Ag nanoparticles (AgNPs) distributing uniformly in TiO_2. The Ag–Carbon–TiO_2 tubes were confirmed high UV–vis light utilization and photocatalytic degradation efficiency to Rhodamine B due to the carbon doping, the surface plasmon resonance of AgNPs and the tubular structure, and the degradation of Rhodamine B reached 90% in 6 h. Meanwhile, they showed an excellent antibacterial effect on staphylococcus aureus, and the fatality rate of Ag–Carbon–TiO_2 tubes to staphylococcus aureus reached 99.9% in 24 h when its concentration was higher than 4 mg/ml. The co-pyrolysis process could repress the AgNPs to grow to be large particles, which could be a key for the excellent antibacterial property. The research showed a promising strategy for preparing Ag–Carbon–TiO_2 composite tubes by co-pyrolysis of PS composite electrospinning fibers, indicating their potential application in wastewater treatment and antibacterial materials.

Graphical Abstract

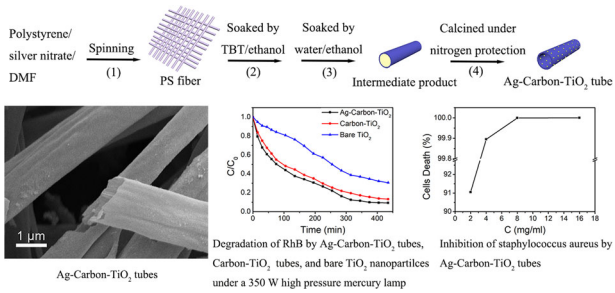

Highlights

- Ag-Carbon-TiO_2 composite tubes are prepared by co-pyrolysis of polystyrene/$AgNO_3$ fibers.
- AgNPs distribute uniformly in C doped TiO_2 due to the co-pyrolysis process.
- The Ag-Carbon-TiO_2 tubes have a thin tube wall without broken or crumbling.
- The size growth of AgNPs can be repressed by the co-pyrolysis process.
- The Ag-Carbon-TiO_2 tubes show excellent antibacterial and oganic degradation properties.

✉ Lijun Ji
ljji@yzu.edu.cn

✉ Guojun Shi
gjshi@yzu.edu.cn

[1] College of Chemistry and Chemical Engineering, Yangzhou University, Yangzhou 225002, China

Keywords Carbon doping · PS fiber · TiO_2 · Ag nanoparticles · Water treatment · Antibacterial property

1 Introduction

Titanium dioxide (TiO_2) is an excellent photocatalyst for degradation of organic pollutants and sterilization of microbial cells due to its excellent properties including high photocatalytic activity, nontoxic, low cost, high stability and no secondary pollution in the degradation process [1, 2]. TiO_2 can produce a large number of electron–hole pairs under the excitation of ultraviolet (UV) light. However, anatase TiO_2 which is a crystalline with the best photocatalytic property can only absorb UV light with a wavelength <400 nm because of its wide band gap (Eg = 3.2 eV), and the UV light excited electrons and holes are easy to recombine. The solar energy utilization of TiO_2 is low. Doping metal or nonmetal elements into TiO_2 has attracted scientists' attention because they find this doping strategy can induce defects into TiO_2, narrowing the band gap, extending the visible light absorption, improving the photocatalytic activity, and solar energy utilization of TiO_2 [3–5].

Doping carbon into TiO_2 or preparing TiO_2/C composite is a popular strategy to prepare TiO_2 photocatalyst of high quantum efficiency [5]. Carbon atom can substitute O atom in TiO_2 lattice and form a series of impurity states in the band gap, which makes the electron–hole pairs possible to be excited by visible light [6]. TiO_2 nanoparticles are often loaded on carbon fibers or carbon nanotubes to form one-dimensional structures, because these kinds of structures can repress the agglomeration of nanoparticles, benefit the transportation of free electrons, and be recycled easily [7, 8].

In recent years, people find that combining silver nanoparticles (AgNPs) with TiO_2 could be a promising choice for preparing TiO_2 photocatalysts. AgNPs are excellent photocatalysts under irradiation of UV light. In addition, AgNPs have been widely applied for water treatment investigation due to their strong antibacterial property [9]. Many researchers have confirmed that the interband transitions and surface plasmon resonance (SPR) effects of AgNPs can improve the UV–vis light absorption of TiO_2 [10–12]. Doping Ag ions into TiO_2 can inhibit the phase transition from anatase to rutile [13], which is beneficial to obtain anatase TiO_2 with excellent photocatalytic performance. For example, AgNPs/TiO_2 composites used for water treatment investigation showed better result than bare TiO_2 [14]. P/Ag/Ag_2O/Ag_3PO_4/TiO_2 photocatalyst was confirmed excellent photocatalytic bactericidal ability [15]. As people do in the field of one-dimensional TiO_2/C composites, one-dimensional TiO_2/Ag composites also attract scientists' attention. Wang et al. prepared Ag/TiO_2 nanofibers by an electrostatic spinning, which showed enhanced photocatalytic property [16]. They speculated that visible light could excite AgNPs and the excited electrons could be transferred into the conductive band of TiO_2 due to the heterostructure of the Ag/TiO_2 nanofibers. Wang et al. prepared AgNPs/TiO_2/graphene nanofibers by an electrostatic spinning [17]. They confirmed that graphene quantum dots could sensitize the AgNPs/TiO_2 composite and improve its photoresponse and photocatalytic activity. In another work, Jiao et al. confirmed that AgNPs/TiO_2/graphene composite nanofibers possessed high photocatalytic efficiency for wastewater treatment and found that the enrichment of organic pollutant on the modified graphene was a key [18]. The hollow structure of TiO_2 nanotubes possesses high specific surface area and can enrich organic pollutant on the surface easily. Bai et al. doped iron, fluorine, and nitrogen into TiO_2 and obtained TiO_2 nanotube arrays exhibiting excellent photocatalytic activity [19]. Ji et al. prepared a carbon-doped TiO_2 nanotube photocatalyst, which indicated excellent activity for decomposing asymmetric dimethylhydrazine [20]. Furthermore, Xiong et al. prepared a Poly (dopamine)/AgNPs/TiO_2 nanotube coating on a Ti implant and achieved excellent in vitro and in vivo bactericidal and biocompatible properties [21]. The uniformly dispersed AgNPs is another key for an excellent antibacterial property. It was confirmed that an Ag/TiO_2 composite film prepared by coating multiple times and uniformly loaded with silver nanoparticles could effectively kill *E. coli* [22].

Since both incorporating metal and nonmetal into TiO_2 showed significant improvement in photocatalytic property, it is highly anticipated that codoping metals and/or nonmetals can create synergistic effects. TiO_2 nanoparticles doped with silver, carbon, and sulfur showed improved photocatalytic property [23]. The improvement was attributed to homogeneous anatase crystalline phase, low band gap, high surface area, and nature of precursor materials. In another work, silver and carbon were doped into titania–silica nanoparticles for investigating their effect on photocatalytic property [24]. The content of silver could be a key for optimizing the photocatalytic properties of TiO_2 composites. A report confirmed that fibrous titania–carbon composite containing 9.5 wt% of silver nanoparticles possessed excellent antibacterial activity [25], and this kind of composite could be used as an anode material [26]. Another report present that Ag/C–TiO_2 nanoparticles loading 0.5–5.0 wt% of silver possessed the best disinfection performance under visible light, compared with a C–TiO_2 sample [27]. A high specific surface area is another key for optimizing the photocatalytic property of TiO_2 composites. Mesoporous titania codoped with carbon and AgNPs

indicated great potential in photocatalytic materials due to its high specific surface area [28]. An investigation showed that depositing silver and tridoping C, N, and S into TiO_2 nanoparticles can significantly enhanced the surface area and improve the photocatalytic property [29]. TiO_2/C composite nanotubes that was loaded with AgNPs and possessed high surface area showed potential for hydrogen generation and organic degradation due to the synergistic effect of carbon layer and surface loaded AgNPs [30]. A titania nanotube array film deposited with carbon quantum dots and AgNPs also present a photocathodic protection effect and could be used as a photoanode [31].

The reported achievements enlightened us that a carbon-doped Ag/TiO_2 tubular structure could be potential for antibacterial and organic degradation application. In this work, we are trying to prepare Ag–Carbon–TiO_2 tubes with excellent photocatalytic efficiency for organic wastewater degradation and bacteria inhibition. We propose that AgNPs can enhance the UV–vis light utilization of TiO_2 through their SPR effect and improve its antibacterial and organic degradation properties, carbon doping can reduce the band gap of TiO_2, thereby improving photocatalytic activity, and the tubular structure can enrich organic pollutant. Polystyrene (PS)/$AgNO_3$ composite fibers prepared by electrospinning are used as templates and carbon source to prepare Ag–Carbon–TiO_2 tubes. This template synthesis strategy has several advantages. Firstly, in most previous work, AgNPs were deposited on TiO_2/carbon composite. In this work, the agglomeration of AgNPs can be repressed and their distribution in the material is uniform because $AgNO_3$ and PS are combined uniformly in advance by dissolving them in a solvent for electrospinning and they will pyrolyze simultaneously in this work, which is conducive to excellent organic degradation and antibacterial properties. Secondly, the obtained Ag–Carbon–TiO_2 tubes can have a thin tube wall without broken or crumbling because carbon, AgNPs, and TiO_2 are combined uniformly and bind tightly in very small size due to the co-pyrolysis process, which is conducive to reuse and also excellent organic degradation and antibacterial properties. Thirdly, only a little carbon residue which is not enough to form a carbon layer can be left and doped into TiO_2 after pyrolysis of PS, so the interior of Ag–Carbon–TiO_2 tubes can enrich and decomposing organic molecules as an active surface, which has advantage over TiO_2 loaded on a material.

2 Experimental

2.1 Preparation of Ag–Carbon–TiO_2 tubes

All the reagents were purchased from Aladdin Industrial Corporation and used as received. A total of 0.05 g silver nitrate and 3 g PS, which was synthesized in our laboratory (Mw = 110,000), were dissolved into 7 g DMF. The mixture was stirred at room temperature for 5 h, and electrospun (16 kV, needle to receiver distance 15 cm, 23 °C) to get $AgNO_3$/PS fibers. The obtained $AgNO_3$/PS fibers were soaked in tetrabutyl titanate for 16 h, and then transferred into a mixture of water/ethanol (1:8 vol/vol) to form $AgNO_3$/PS/TiO_2 composite fibers. After calcinations at 450 °C for 2 h under nitrogen, Ag–Carbon–TiO_2 composite tubes were obtained. In the control experiment, Carbon–TiO_2 composite tubes were prepared by a similar process without dissolving silver nitrate in DMF. Anatase TiO_2 nanoparticles purchased from Aladdin Industrial Corporation were also used as control without any further treatment.

2.2 Characterization of materials

The observation and analysis of the morphology, structure, and composition of the samples were performed by a scanning electron microscope (SEM, Gemini, 300) and a high-resolution transmission electron microscope (HRTEM, Tecnai, G2 F30). X-ray diffraction (XRD) patterns of all samples were acquired on a Bruker AXS D8 ADVANCE X-ray diffractometer to confirm the phase composition. BET-specific surface area and pore size distribution were measured by a Bei Shi De 3H-2000PS2 instrument. Raman spectra were obtained by a Renishaw Raman spectrometer. The thermal stability of the samples was characterized by thermal gravity analysis (TGA, PerkinElmer). The analysis of UV–vis–NIR spectra of the samples were carried out on a Cary 5000 spectrophotometer. UV–vis absorption was characterized by a PerkinElmer Lambda 950 spectrophotometer. Transient photocurrent response was measured using an electrochemical workstation (CHI 660E, Shanghai Chenhua Instruments) with a 40 W incandescent lamp as a light source and an aqueous solution Na_2SO_4 (0.1 mol/l) as an electrolyte solution. The working electrodes were prepared by coating 10 mg of samples on indium tin oxide conductive glasses (2 × 1 cm). The counter electrode was a platinum sheet electrode, and the reference electrode was a calomel electrode.

2.3 Photocatalytic activity

Photocatalyst powder (30 mg) was dispersed in an aqueous solution of 25 ml Rhodamine B (RhB) (20 mg/l), and the performance of the catalysts was measured by a 350 W high-pressure mercury lamp on a photocatalytic apparatus (YM-GHX-1 Shanghai Yu Ming Yi Qi co. LTD). One milliliter of degraded RhB solution was added to a volumetric flask of 5 ml, and then diluted to the scale to obtain the sample. A UV spectrophotometer was used to measure the absorbance of the sample, and the degradation rate of RhB in aqueous solution was calculated according to the equation: Degradation (%) =

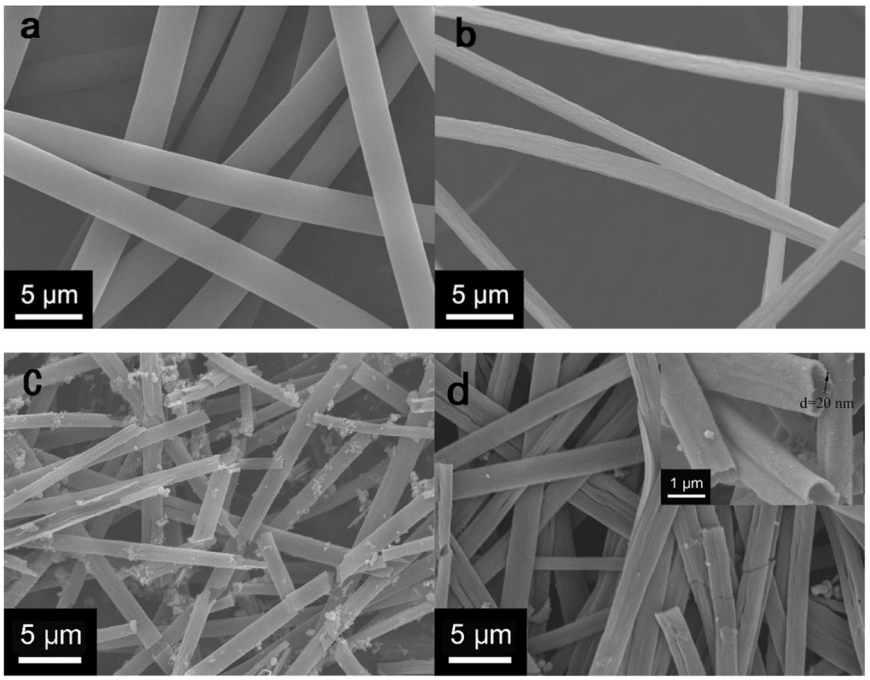

Fig. 1 **a** PS fibers prepared with a PS electrospun solution of 30 wt%. **b** $AgNO_3$/PS composite fibers showed smaller diameter than PS fibers. **c** Carbon–TiO_2 tubes prepared by loading TiO_2 on PS fibers and calcinations. **d** Ag–Carbon–TiO_2 tubes prepared by loading TiO_2 on $AgNO_3$/PS fibers and calcinations

$(C_0 - C_t)/C_0 \times 100\%$, in which C_0 and C_t were the initial and the tested concentration, respectively.

2.4 Evaluation of antibacterial activity

The evaluation of antibacterial activity was carried out according to a national food safety standard of China (GB 4789.10-2016) and reported references [32, 33]. To determine the inhibition of staphylococcal growth by antibacterial agents, 0.2 ml of Staphylococcus aureus was added into 4.8 ml of LB medium, and different quantitative antibacterial agents were added. The samples were then placed in a 37 °C incubator for 12 h. The obtained bacterial suspensions were diluted to make 10^{-1}, 10^{-2}, 10^{-3}, 10^{-4}, 10^{-5}, 10^{-6}, 10^{-7}, 10^{-8}, 10^{-9}, 10^{-10}, 10^{-11}, 10^{-12}, 10^{-13}, 10^{-14}, and 10^{-15} diluents, and then 50 μl of the diluents were evenly spread on the blood agar medium for bacterial culture at 37 °C for 24 h. The number of the colonies on the plates was converted to the number of viable cells in the original bacterial solution based on the diluents of the bacterial suspension and the amount of liquid applied to the plate.

3 Results and discussions

3.1 Characterization

The diameter of PS fibers prepared by a PS DMF solution of 30 wt% was about 3 μm with a narrow size distribution (Fig. 1a). When $AgNO_3$ was added into the electrospun solution, the fiber diameter decreased to 1–2 μm, and the fiber surface became rough (Fig. 1b). The reason could be that the conductivity of the electrospinning solution mixed with $AgNO_3$ increased comparing with a PS DMF solution, which resulted in high electric field intensity [16]. High electric field intensity offered high surface tension, which stretched the fibers to be thinner. By the sol–gel method, TiO_2 formed on the surface of the PS/$AgNO_3$ or PS fibers. PS/$AgNO_3$/TiO_2 composite fibers and PS/TiO_2 composite fibers all became tubular structures after calcinations in nitrogen atmosphere because the PS fibers were pyrolyzed and left only a little carbon residue (Fig. 1c, d). The surface of the Ag–Carbon–TiO_2 composite tubes was smooth with only a small amount of titania particles distributing sparsely on tubes, suggesting that AgNPs did not agglomerate in the sintering process. The wall thickness of the Ag–Carbon–TiO_2 tubes was about 20 nm. Tubes with thinner wall could possess higher specific surface area and photocatalytic activity, which was conducive to the adsorption and degradation of organic molecules.

High-angle annular dark field imaging indicated that Ti, O, and Ag signals distributed uniformly throughout the Ag–Carbon–TiO_2 tubes, confirming the SEM result that AgNPs did not agglomerate in the sintering process and dispersed uniformly in TiO_2 phase. The aggregation of silver nanoparticles may lead to a decrease in SPR effect, thereby reducing photocatalyticand antibacterial efficiencies (Fig. 2).

It was observed by HRTEM that the Ag–Carbon–TiO_2 tubes were composed of nanocrystals of TiO_2 and graphite carbon, amorphous carbon and AgNPs. These components

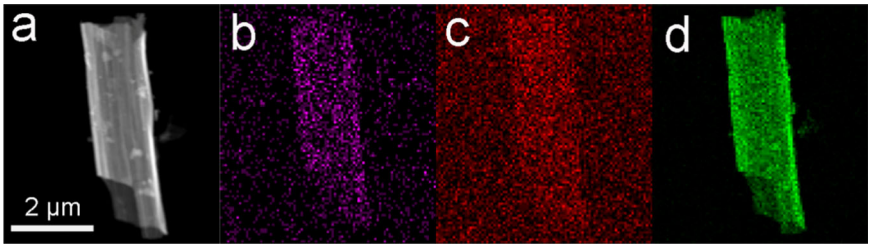

Fig. 2 **a** HAADF image of Ag–Carbon–TiO_2, and its element mappings of (**b**) Ag, (**c**) oxygen, and (**d**) titanium

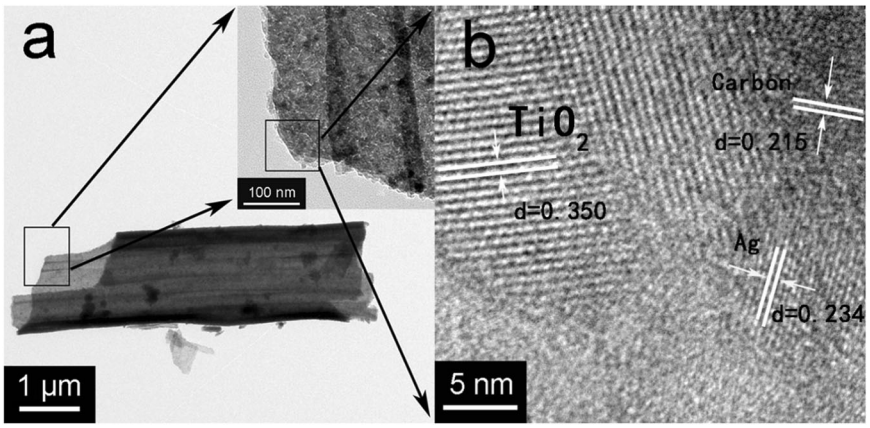

Fig. 3 HRTEM images of The Ag–Carbon–TiO_2 tube formed after calcining

were distributed uniformly throughout the tubes. The AgNPs presented an average size of 20–30 nm and a lattice spacing of 0.234 nm. The lattice spacing of 0.350 nm can be assigned to the (101) plane of anatase TiO_2 [34]. The carbon nanocrystals present an average size of about 5–10 nm with a lattice spacing of 0.215 nm. Since the size of the carbon nanocrystals was small, their ordered crystalline structure was not as clear as anatase TiO_2 and AgNPs (Fig. 3).

An increase of about 2 wt% in weight was found in the TGA pattern of the sample Ag–Carbon–TiO_2 tubes in air flow when temperature increased from 40 to 200 °C, which can be attributed to the oxidation of AgNPs. When the temperature reached 250 °C, silver oxide started to decompose. The Ag–Carbon–TiO_2 tubes indicated a loss of 4 wt% in air flow when the temperature was increased to 650 °C, This weight loss could be due to the oxidation of carbon component in the Ag–Carbon–TiO_2 tubes. The results showed that the Ag–Carbon–TiO_2 tubes had an AgNPs content of about 0.5 wt%, a TiO_2 content of about 95.5 wt%, and a carbon content of about 4 wt%. EDS characterization indicated a consistent result (Table 1 and Fig. 4).

Figure 5a showed the XPS spectrum of the Ag–Carbon–TiO_2 tubes. The coexistence of Ti, O, C, and Ag elements in Ag–Carbon–TiO_2 tubes could be determined by the XPS spectra. Ag $3d_{5/2}$ peak appeared at the binding energy of 367.8 eV; Ag $3d_{3/2}$ peak appeared at the binding energy of 373.8 eV, and the difference between the two peaks was 6.0 eV (Fig. 5b). Comparing with the two peaks of metallic silver at 374.1 and 368.1 eV [35], the two

Table 1 The EDS result confirms the composition of the Ag–Carbon–TiO_2 tubes

Element names	Ti	C	Ag	Mean content of Ag
Atomic percent (%)	65.19	34.48	0.33	
	65.31	34.41	0.28	
	69.00	30.78	0.22	0.252 mol.%
	65.95	33.78	0.26	0.481%
	65.25	34.58	0.17	

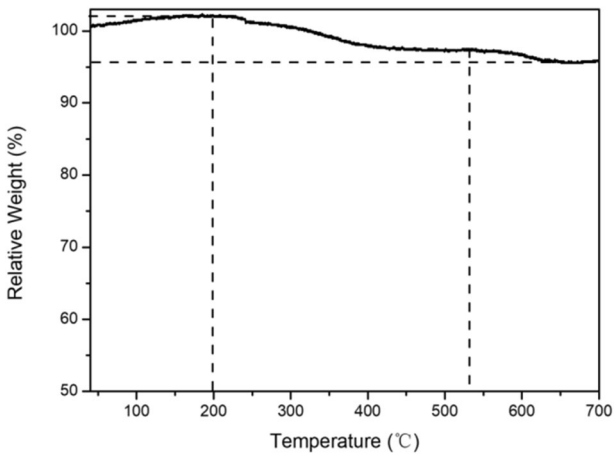

Fig. 4 TGA confirmed the existence of carbon

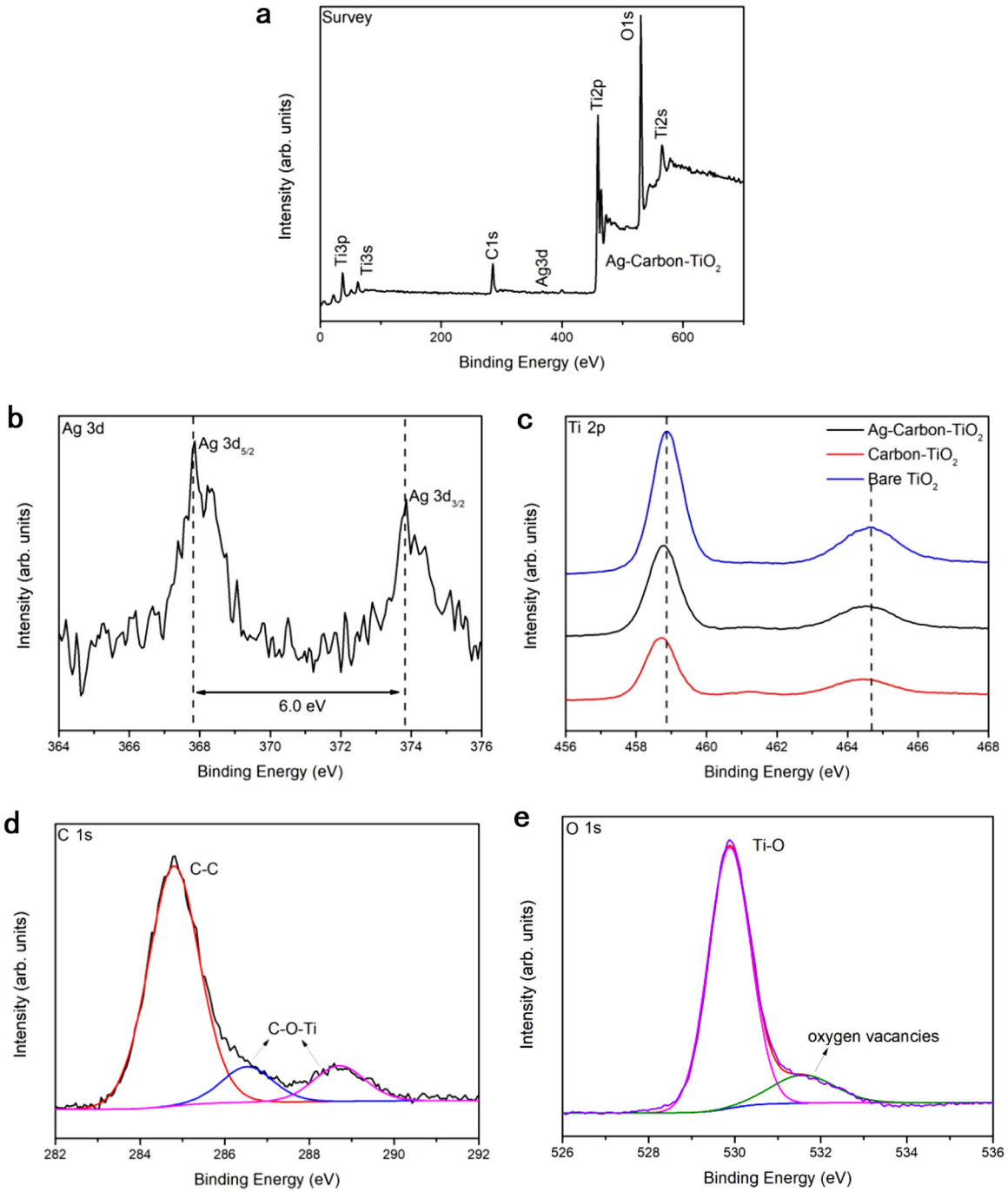

Fig. 5 XPS spectra of the Ag–Carbon–TiO_2 tubes: **a** The survey spectra; **b** Ag 3d; **c** Ti 2p; **d** C 1s and **e** O 1s

Ag 3d peaks of the Ag–Carbon–TiO_2 tubes moved to lower binding energy. The reason could be that the tiny AgNPs formed following the pyrolysis of PS/$AgNO_3$ fibers embedded into TiO_2, forming Ag–TiO_2 heterostructure with large interface. The zero-valent silver on the interface was converted into univalent silver. Since the binding energy of univalent silver was lower than that of zero-valent silver, the peaks of the sample moved to low binding energy [11]. The Ti $2p_{3/2}$ and Ti $2p_{1/2}$ peaks of bare TiO_2 were at 458.88 and 464.63 eV with a split gap 5.7 eV (Fig. 5c), confirming that the valence state of titanium was +4 [36]. The Carbon–TiO_2 showed a binding energy of Ti $2p_{3/2}$ at 458.73, 0.15 eV lower than that of bare TiO_2, while Ag–Carbon–TiO_2 exhibited a binding energy of Ti $2p_{3/2}$ at 458.78, 0.10 eV lower than that of bare TiO_2. These shifts were attributed to the strong interaction between Ti^{4+} and

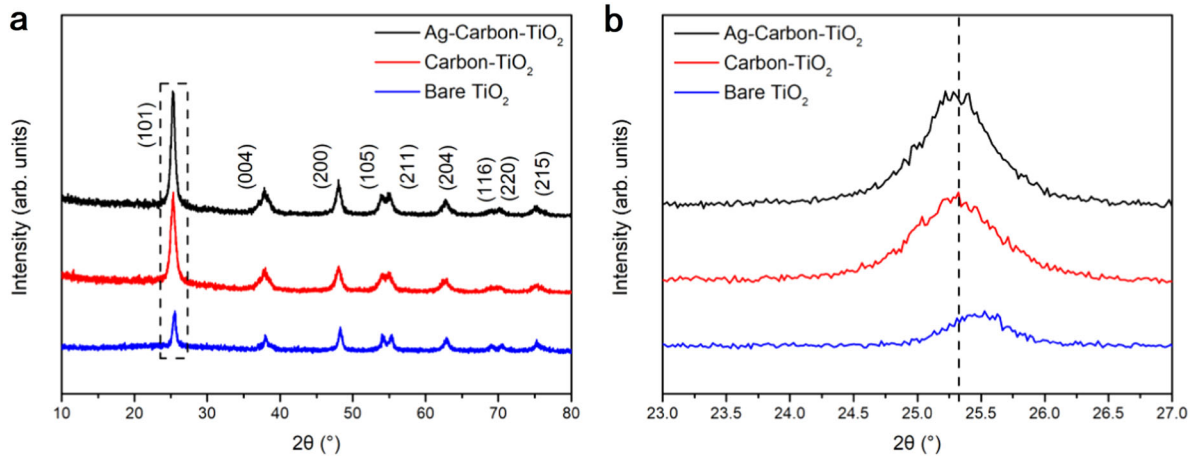

Fig. 6 XRD spectra of Ag–Carbon–TiO_2, Carbon–TiO_2 and bare TiO_2. **b** Is the partial enlarged view of **a**

carbon [4]. Figure 5d showed that the high-resolution spectrum of C 1s consisted of three peaks at 284.9, 286.7, and 288.8 eV. The peak centered at 284.9 eV could be attributed to the C–C bond of carbon quantum dots (Fig. 3b), which were sensitizers enhancing the visible light response of TiO_2 [37, 38]. Figure 5e showed the binding energy of O 1s. The Ti–O bond was at 529.89 eV, and the peak at 518.82 eV belonged to the oxygen vacancy, which improved the photocatalytic activity [39].

Figure 6a showed that TiO_2 in Ag–Carbon–TiO_2 composites, Carbon–TiO_2 composites, and bare TiO_2 was all anatase, which was characterized with (101), (004), (200), (105) plane diffraction around 2θ (25.3°), (37.9°), (48.0°), (53.9°). The diffraction peak of Ag was not found in the sample because the concentration of Ag in the sample was very low. Figure 6b showed a magnified diffraction region of the sample between 23 and 28°. It indicated that the peaks of (101) planes of the Ag–Carbon–TiO_2 tubes and Carbon–TiO_2 tubes shift to lower 2θ direction, comparing with the corresponding peak of bare TiO_2. The shift could be due to carbon doping in the sample [40]. The radius of oxygen atom was smaller than that of carbon atom, and Ti–C bond length was longer than Ti–O bond. Carbon atoms substitute oxygen atoms in the crystal lattice, leading to distortion of TiO_2 lattice [41].

A Raman spectrum of Ag–Carbon–TiO_2 composite tubes showed four strong peaks at 152, 403, 517, and 640 cm^{-1}, which corresponded to the peaks of $E_{g(1)}$, $B_{1g(1)}$, $A_{1g} + B_{1g(2)}$, and $E_{g(3)}$ of anatase TiO_2 [42]. Two extra peaks belonged to D band and G band of carbon appeared at 1360 and 1590 cm^{-1}. The intensity of D band and G band (I_D: I_G) can be used to measure the graphitization degree of carbon materials [43]. The I_D: I_G of the Ag–Carbon–TiO_2 composite tubes was 1.09, suggesting that considerable amounts of amorphous carbon and crystalline carbon co-exist in TiO_2 (Fig. 7).

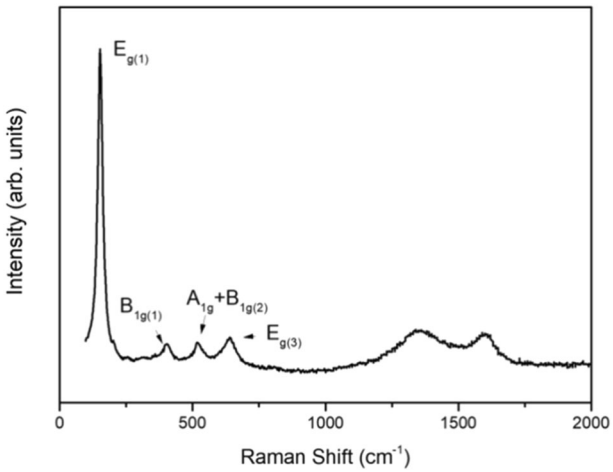

Fig. 7 A Raman spectrum of the Ag–Carbon–TiO_2 tubes

Figure 8 showed the nitrogen adsorption/desorption isotherms and corresponding pore size curves of Ag–Carbon–TiO_2, Carbon–TiO_2 and bare TiO_2. The pore size distributions of all three samples were polydispersed and similar. The specific surface area of Ag–Carbon–TiO_2 was 45.8 $m^2 g^{-1}$, which was not very large because the tubular structure had little nanoscale pores (Fig. 8a). The nitrogen adsorption/desorption isotherms of Ag–Carbon–TiO_2, Carbon–TiO_2, and bare TiO_2 belonged to type IV in IUPAC classification, showing the characteristics of macroporous structures.

3.2 Photocatalytic organic degradation and antibacterial properties

Figure 9 recorded the UV–vis absorption spectra of Ag–Carbon–TiO_2, Carbon–TiO_2, and bare TiO_2. In 220–800 nm range, the absorption strength of bare TiO_2,

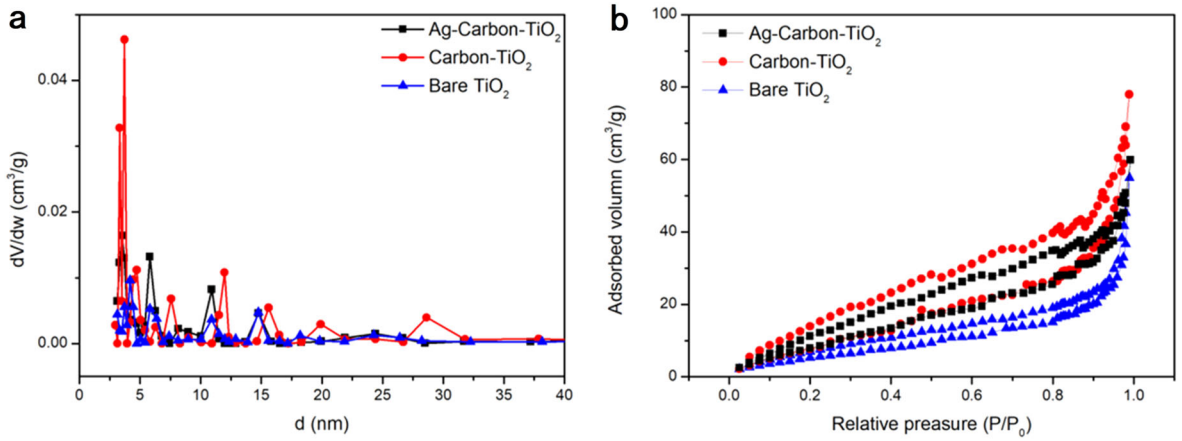

Fig. 8 **a** The pore size distribution of the sample Ag–Carbon–TiO_2, Carbon–TiO_2, and bare TiO_2. **b** The corresponding nitrogen adsorption/desorption isotherms

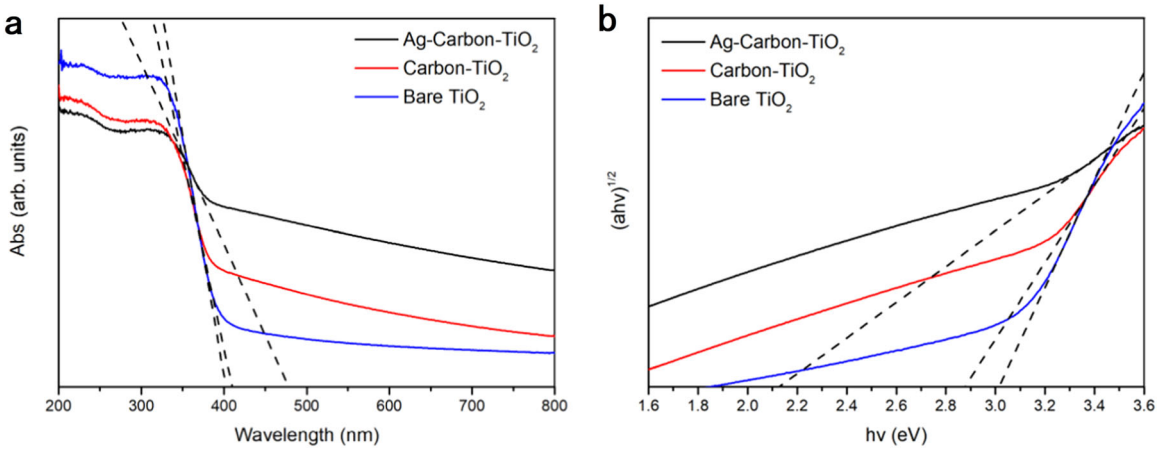

Fig. 9 **a** and **b** are the UV absorption spectra and band gap energies of Ag–Carbon–TiO_2, Carbon–TiO_2, and bare TiO_2

Carbon–TiO_2 tubes, and Ag–Carbon–TiO_2 tubes increased in turn. The Ag–Carbon–TiO_2 tubes showed the strongest absorption of UV–vis light because they had both carbon doping and AgNPs SPR effects. Compared with bare TiO_2, which absorbed UV–vis light up to 400 nm, the Carbon–TiO_2 tubes absorbed light up to 410 nm, and the Ag–Carbon–TiO_2 tubes extended from 400 to 470 nm. The band gap energies of bare TiO_2, Carbon–TiO_2 tubes and Ag–Carbon–TiO_2 tubes calculated by Kubelka–Munk rule were 3.02, 2.89, and 2.12 eV, respectively [44]. It confirmed that carbon doping and AgNPs led to the reduction of the band gap width, which was consistent with the reported results [6, 10]. Therefore, the Ag–Carbon–TiO_2 tubes should possess the best photocatalytic property [45, 46].

The photoelectron transfer efficiency of the Carbon–TiO_2 tubes and Ag–Carbon–TiO_2 tubes were investigated by measuring their instantaneous photocurrent. Carbon–TiO_2 tubes and Ag–Carbon–TiO_2 tubes expressed fast and repeatable transient response currents under intermittent

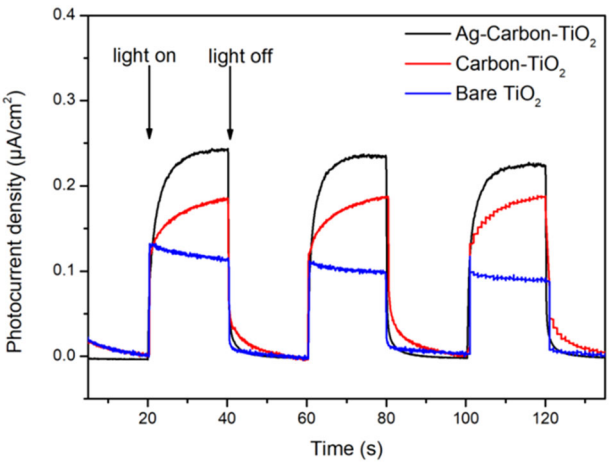

Fig. 10 The transient photocurrent response curves of Ag–Carbon–TiO_2 tubes, Carbon–TiO_2 tubes, and bare TiO_2

visible light. The transient response current of Ag–Carbon–TiO_2 tubes was stronger than that of Carbon–TiO_2 tubes, which could be attributed to the local SPR effect of AgNPs [47]. The results suggested that Ag–Carbon–TiO_2 tubes had higher photogenic electron–hole pair separation efficiency and electron transfer efficiency, which improved the photocatalytic performance (Fig. 10).

By degrading RhB, it was confirmed that the Ag–Carbon–TiO_2 tubes had excellent photocatalytic activity. The bare TiO_2 and Carbon–TiO_2 tubes were also used to decompose RhB for comparison. Under the irradiation of mercury lamps, the concentration of RhB in the mixture solution of Ag–Carbon–TiO_2 tubes decreased about 90% in 6 h, while the concentration of the samples of bare TiO_2 and Carbon–TiO_2 tubes decreased relatively slow, with the degradation rate of about 62 and 82% (Fig. 11). The enhanced photocatalytic activity of the Ag–Carbon–TiO_2 tubes was caused by carbon doping and the presence of AgNPs.

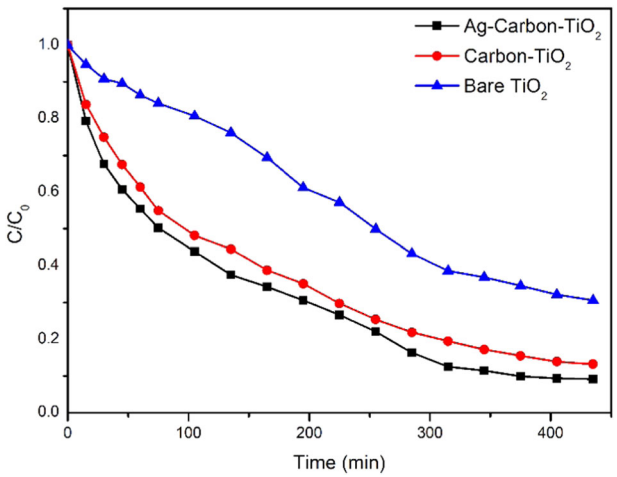

Fig. 11 Degradation curve of Ag–Carbon–TiO_2 tubes, Carbon–TiO_2 tubes, and bare TiO_2 to RhB

The inhibition of bacterial growth by TiO_2 could be improved by the addition of AgNPs. As shown in Fig. 12a–d, staphylococcus aureus stopped growing in diluents of 10^{-11}, 10^{-9}, 10^{-7}, and 10^{-5} with different concentrations of the bacteriostatic agents. As the concentration of the bacteriostatic agent increases (Fig. 12e), the antibacterial effect was significantly improved. The results showed that the antibacterial activity of Ag–Carbon–TiO_2 composite reached 99.9% when its concentration was higher than 4 mg/ml.

Based on the experimental facts and analysis, the high photocatalytic antibacterial and organic degradation properties of the Ag–Carbon–TiO_2 tubes could be explained by the composition and structure of the material [20, 32, 33]. Carbon formed impurity levels in TiO_2 shell, as being confirmed by the XPS spectrum and the XRD mode. The impurity levels made TiO_2 easy to be activated by the light source of mercury lamp. When charges were separated under the irradiation of light, the generated photoelectrons were transferred into the TiO_2 conduction band, and then captured by AgNPs. AgNPs can also effectively improve their photocatalytic activity against visible light because of the SPR induced by surface electron collective oscillation [44, 48]. The SPR of AgNPs located in the visible region, which could improve the absorption intensity of visible

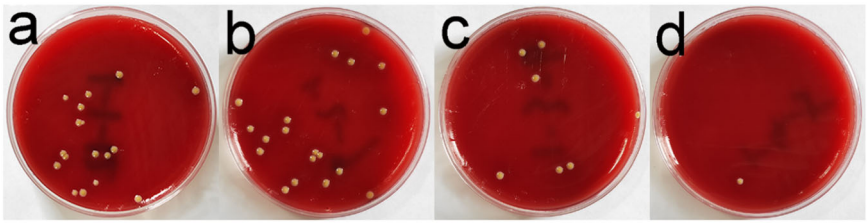

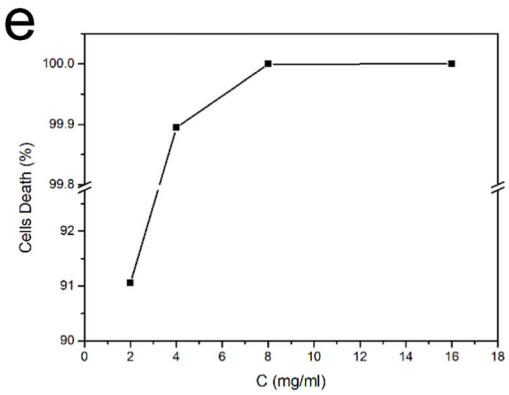

Fig. 12 The **a**–**d** were blood AGAR media obtained with 2, 4, 8, and 16 mg/ml bacteriostatic agents. The **e** was the fatality rate of Ag–Carbon–TiO_2 to staphylococcus aureus at different concentrations

light and reduce the band gap width [49], as confirmed by the UV–vis absorption spectra in Fig. 9. Meanwhile, the h^+ produced by the AgNPs could directly oxidize organic molecules. Therefore, the photocatalytic activity of the Ag–Carbon–TiO_2 tubes remained at a high level, and its rapid degradation performance was attributed to the unique microstructure [50, 51]. The long tubular structure of the Ag–Carbon–TiO_2 composite increased their contact chance with bacteria [32], resulting in more cell membrane damage and inhibiting bacterial growth. The bacteriostatic activity of a carbon- and Ag-doped TiO_2 could also be significantly improved by the relative higher surface area of the tubular structure because a higher surface area could increase the reactivity of the crystal surface [33]. The augment of oxygen deficiency increased the damage to the cell wall and the permeability of the cell membrane. The presence of abundant oxygen defects increased intracellular oxidative stress and could cause damage to intracellular systems, such as cell membranes, DNA, and proteins.

4 Conclusion

To sum up, we had designed a co-pyrolysis method of silver nitrate/PS fiber/TiO_2 composite to prepare Ag–Carbon–TiO_2 composite tubes. The diameter of the Ag–Carbon–TiO_2 composite tubes was about 2 μm, and the tube wall was composed of anatase-TiO_2, AgNPs, amorphous carbon, crystalline carbon, and carbon elements doped into TiO_2 lattice. The outstanding photocatalytic antibacterial and organic degradation properties of the Ag–Carbon–TiO_2 composite tubes were attributed to the reduction of the TiO_2 band gap energy, the improvement of visible light utilization, and the inhibition of charge recombination. The co-pyrolysis process ensured that AgNPs with a diameter of about 20 nm could distribute uniformly in TiO_2 to form a heterogeneous structure, which was a key for repressing the agglomeration of AgNPs. In addition, as PS composite fibers were easy to be prepared by co-electrospinning, this work suggested that TiO_2 tubes containing other materials could be prepared by the same way.

Acknowledgements This work was supported by the Natural Science Foundation of Jiangsu Province (No. BK20131226), the National Natural Science Foundation of China (Nos. 51273171 and 51673090), and a project funded by the Priority Academic Program Development of Jiangsu Higher Education Institutions.

Compliance with ethical standards

Conflict of interest The authors declare that they have no conflict of interest.

References

1. Komatsuda S, Asakura Y, Vequizo JJM et al. (2018) Enhanced photocatalytic NO decomposition of visible-light responsive F-TiO2/(N,C)-TiO2 by charge transfer between F-TiO2 and (N,C)-TiO2 through their doping levels. Appl Catal B 238:358–364
2. Matsunaga T, Tomoda R, Nakajima T, Wake H (1985) Photochemical sterilization of microbial cells by semiconductor powders. FEMS Microbiol Lett 29:211–214
3. Xie A, Zhou X, Zhou W et al. (2016) Preparation and enhanced photocatalytic activity of S-doped TiO2/palygorskite composites. Mater Technol 322:65–271
4. Ksibi M, Rossignol S, Tatibouët JM, Trapalis C (2008) Synthesis and solid characterization of nitrogen and sulfur-doped TiO2 photocatalysts active under near visible light. Mater Lett 62:4204–4206
5. Jaiswal R, Bharambe J, Patel N et al. (2015) Copper and nitrogen co-doped TiO2 photocatalyst with enhanced optical absorption and catalytic activity. Appl Catal B 168-169:333–341
6. Yu H, Shi R, Zhao Y et al. (2016) Smart utilization of carbon dots in semiconductor photocatalysis. Adv Mater 28:9454–9477
7. Valentin D, Cristiana, Pacchioni G, Selloni A (2005) Theory of carbon doping of titanium dioxide. Chem Mater 17:6656–6665
8. Rim AH, HyeLa A, Byoung KW, Jin AH (2014) Nitrogen-doped TiO2 nanoparticle-carbon nanofiber composites as a counter electrode for Pt-free dye-sensitized solar cells. ECS Solid State Lett 3:33–36
9. Taha Aboueloyoun A (2015) Direct synthesis of mesostructured carbon nanofibers decorated with silver-nanoparticles as a multifunctional membrane for water treatment. Adv Nat Sci 6:045003
10. Wang Y, Yan C, Chen L et al. (2017) Controllable charge transfer in Ag-TiO2 composite structure for sers application. Nanomaterials 7:159
11. Jbeli A, Hamden Z, Bouattour S et al. (2018) Chitosan-Ag-TiO2 films: an effective photocatalyst under visible light. Carbohydr Polym 199:31–40
12. Fei J, Li J (2015) Controlled preparation of porous TiO2-Ag nanostructures through supramolecular assembly for plasmon-enhanced photocatalysis. Adv Mater 27:314–319
13. Yu J, Xiong J, Cheng B, Liu S (2005) Fabrication and characterization of Ag–TiO2 multiphase nanocomposite thin films with enhanced photocatalytic activity. Appl Catal B 60:211–221
14. Zhao T, Xing Z, Xiu Z et al. (2019) Synergistic effect of surface plasmon resonance, Ti(3+) and oxygen vacancy defects on Ag/MoS2/TiO2-x ternary heterojunctions with enhancing photothermal catalysis for low-temperature wastewater degradation. J Hazard Mater 364:117–124
15. Liu N, Zhu Q, Zhang N et al. (2019) Superior disinfection effect of Escherichia coli by hydrothermal synthesized TiO2-based composite photocatalyst under LED irradiation: Influence of environmental factors and disinfection mechanism. Environ Pollut 247:847–856
16. Wang Y, Liu L, Xu L et al. (2013) Ag/TiO2 nanofiber heterostructures: Highly enhanced photocatalysts under visible light. J Appl Phys 113:174311
17. Wang W, Wang S, Lv J et al. (2018) Enhanced photoresponse and photocatalytic activities of graphene quantum dots sensitized Ag/TiO2 thin film. J Am Ceram Soc 101:5469–5476
18. Liu Y, Hou C, Jiao T et al. (2018) Self-assembled AgNP-containing nanocomposites constructed by electrospinning as efficient

dye photocatalyst materials for wastewater treatment. Nanomaterials 8:35
19. Hua Z, Dai Z, Bai X et al. (2015) A facile one-step electrochemical strategy of doping iron, nitrogen, and fluorine into titania nanotube arrays with enhanced visible light photoactivity. J Hazard Mater 293:112–121
20. Ji L, Zhang Y, Miao S et al. (2017) In situ synthesis of carbon doped TiO2 nanotubes with an enhanced photocatalytic performance under UV and visible light. Carbon 125:544–550
21. Gao C, Cheng H, Xu N et al. (2019) Poly(dopamine) and Ag nanoparticle-loaded TiO2 nanotubes with optimized antibacterial and ROS-scavenging bioactivities. Nanomedicine 14:803–818
22. Zhu Q, Hu X, Stanislaus MS et al. (2017) A novel P/Ag/Ag2O/Ag3PO4/TiO2 composite film for water purification and antibacterial application under solar light irradiation. Sci Total Environ 577:236–244
23. Hamal DB, Klabunde KJ (2007) Synthesis, characterization, and visible light activity of new nanoparticle photocatalysts based on silver, carbon, and sulfur-doped TiO2. J Colloid Interface Sci 311:514–522
24. Chen Q, Shi H, Shi W et al. (2012) Enhanced visible photocatalytic activity of titania–silica photocatalysts: effect of carbon and silver doping. Catal Sci Technol 2:1213–1220
25. Liu X, Luo Y, Wu T, Huang J (2012) Antibacterial activity of hierarchical nanofibrous titania–carbon composite material deposited with silver nanoparticles. N J Chem 36:2568–2573
26. Li S, Huang J (2015) A nanofibrous silver-nanoparticle/titania/carbon composite as an anode material for lithium ion batteries. J Mater Chem A 3:4354–4360
27. Zhang L, Han M, Tan OK et al. (2013) Facile fabrication of Ag/C-TiO2 nanoparticles with enhanced visible light photocatalytic activity for disinfection of Escherichia coli and Enterococcus faecalis. J Mater Chem B 1:564–570
28. Qiang L, Zhi-Bo Z, Chang-Qing D et al. (2014) Improved visible-light photocatalytic activity of bi-crystalline mesoporous titania codoped with carbon and silver. Int J Inorg Mater 29:1333–1338
29. Jabbari V, Hamadanianm, Karimzadeh S, Villagrán D (2016) Enhanced charge carrier efficiency and solar light-induced photocatalytic activity of TiO2 nanoparticles through doping of silver nanoclusters and C–N–S nonmetals. J Ind Eng Chem 35:132–139
30. Zhang X, Ge M, Dong J et al. (2019) Polydopamine-inspired esign and synthesis of visible-light driven Ag NPs@C@elongated TiO2 NTs core−shell nanocomposites for sustainable hydrogen generation. ACS Sustain Chem Eng 7:558–568
31. Guan Z, Jin P, Liu Q et al. (2019) Carbon quantum dots/Ag sensitized TiO2 nanotube film for applications in photocathodic protection. J Alloy Compd 797:912–921
32. Mohammad MR, Ahmed DS, Mohammed MKA (2019) Synthesis of Ag-doped TiO2 nanoparticles coated with carbon nanotubes by the sol–gel method and their antibacterial activities. J Sol-Gel Sci Technol 90:498–509
33. Haider AJ, Mohammed MR, Al-Mulla EAJ, Ahmed DS (2014) Synthesis of silver nanoparticle decorated carbon nanotubes and its antimicrobial activity against growth of bacteria. Rendiconti Lincei 25:403–407
34. Cheng C, Tan X, Lu D et al. (2015) Carbon-dot-sensitized, nitrogen-doped TiO2 in mesoporous silica for water decontamination through nonhydrophobic enrichment-degradation mode. Chemistry 21:17944–17950
35. Yang G, Yin H, Liu W et al. (2018) Synergistic Ag/TiO2-N photocatalytic system and its enhanced antibacterial activity towards acinetobacter baumannii. Appl Catal B 224:175–182
36. Mohamed MA, Salleh WNW, Jaafar J et al. (2017) Carbon as amorphous shell and interstitial dopant in mesoporous rutile TiO2: bio-template assisted sol-gel synthesis and photocatalytic activity. Appl Surf Sci 393:46–59
37. Xing M, Zhang J, Chen F, Tian B (2011) An economic method to prepare vacuum activated photocatalysts with high photoactivities and photosensitivities. Chem Commun 47:4947–4949
38. Shao J, Sheng W, Wang M et al. (2017) In situ synthesis of carbon-doped TiO2 single-crystal nanorods with a remarkably photocatalytic efficiency. Appl Catal B 209:311–319
39. Yao L, Wang W, Liang Y et al. (2019) Plasmon-enhanced visible light photoelectrochemical and photocatalytic activity of gold nanoparticle-decorated hierarchical TiO2/Bi2WO6 nanorod arrays. Appl Surf Sci 469:829–840
40. Wu X, Yin S, Dong Q et al. (2013) Synthesis of high visible light active carbon doped TiO2 photocatalyst by a facile calcination assisted solvothermal method. Appl Catal B 142-143:450–457
41. Liu J, Zhu W, Yu S, Yan X (2014) Three dimensional carbogenic dots/TiO2 nanoheterojunctions with enhanced visible light-driven photocatalytic activity. Carbon 79:369–379
42. Li M, Lu B, Ke Q et al. (2017) Synergetic effect between adsorption and photodegradation on nanostructured TiO2/activated carbon fiber felt porous composites for toluene removal. J Hazard Mater 333:88–98
43. Yang C, Zhang X, Qin J et al. (2017) Porous carbon-doped TiO2 on TiC nanostructures for enhanced photocatalytic hydrogen production under visible light. J Catal 347:36–44
44. Ge M, Cao C, Li S et al. (2016) In situ plasmonic Ag nanoparticle anchored TiO2 nanotube arrays as visible-light-driven photocatalysts for enhanced water splitting. Nanoscale 8:5226–5234
45. Zhang Y, Gong M, Liu X et al. (2018) Preparation of activated carbon nanotube foams loaded with Ag-doped TiO2 for highly efficient photocatalytic degradation under UV and visible light. J Mater Sci 54:2975–2989
46. Scott T, Zhao H, Deng W et al. (2019) Photocatalytic degradation of phenol in water under simulated sunlight by an ultrathin MgO coated Ag/TiO2 nanocomposite. Chemosphere 216:1–8
47. Wang X, Xiang Y, Zhou B et al. (2019) Enhanced photocatalytic performance of Ag/TiO2 nanohybrid sensitized by black phosphorus nanosheets in visible and near-infrared light. J Colloid Interface Sci 534:1–11
48. Chaudhary D, Singh S, Vankar VD, Khare N (2017) A ternary Ag/TiO2/CNT photoanode for efficient photoelectrochemical water splitting under visible light irradiation. Int J Hydrog Energy 42:7826–7835
49. Mandari KK, Kwak BS, Police AKR, Kang M (2017) In-situ photoreduction of silver particles and their SPR effect in enhancing the photocatalytic water splitting of Ag2O/TiO2 photocatalysts under solar light irradiation: a case study. Mater Res Bull 95:515–524
50. Liu Y, Xu G, Lv H (2018) Ag modified Fe-doping TiO2 nanoparticles and nanowires with enhanced photocatalytic activities for hydrogen production and volatile organic pollutant degradation. J Mater Sci 29:10504–10516
51. Li X, Gao Y, Liu J et al. (2017) Facile synthesis of Ti3+ doped Ag/AgI-TiO2 nanoparticles with efficient visible-light photocatalytic activity. Int J Hydrog Energy 42:13031–13038